RAA 2015 Vol. **15** No. **1**, 64–76 doi: 10.1088/1674–4527/15/1/007
http://www.raa-journal.org *http://www.iop.org/journals/raa*

Research in Astronomy and Astrophysics

Study of a solar flare on 2005 August 22 observed in hard X-rays and microwaves *

Zhong-Yin Liu[1], You-Ping Li[1], Wei-Qun Gan[1] and Kazi A. Firoz[2]

[1] Key Laboratory of Dark Matter and Space Astronomy, Purple Mountain Observatory, Chinese Academy of Sciences, Nanjing 210008, China; *liuzy@pmo.ac.cn*
[2] Space Research Group, Alcala University, 28871 Alcala de Henares, Spain

Received 2014 March 11; accepted 2014 May 5

Abstract We investigate the 2005 August 22 flare event (00:54 UT) exploiting hard X-ray (HXR) observations from the *Reuven Ramaty High Energy Solar Spectroscopic Imager* (*RHESSI*) and microwave (MW) observations from the Nobeyama Solar Radio Observatory. The HXR time profile exposes well-damped quasi-periodic pulsations with four sequential peaks, and the MW time profile follows the corresponding peaks. Based on this feature, we derive the time relationship of HXRs and MWs with multi-frequency data from the Nobeyama Radio Polarimeter, and the spatially resolvable data from *RHESSI* and the Nobeyama Radioheliograph. We find that both frequency dependent delays in MWs and energy dependent delays in HXRs are significant. Furthermore, MW emissions from the south source are delayed with respect to those from the north source at both 17 GHz and 34 GHz, but no significant delays are found in HXR emissions from the different sources at the same energies. To better understand all these long time delays, we derive the electron fluxes of different energies by fitting the observed HXR spectra with a single power-law thick-target model, and speculate that these delays might be related to an extended acceleration process. We further compare the time profile of a MW spectral index derived from 17 and 34 GHz fluxes with the flux densities, and find that the spectral index shows a strong anti-correlation with the HXR fluxes.

Key words: Sun: flares — Sun: radio radiation — Sun: X-rays, gamma rays

1 INTRODUCTION

Emissions of hard X-rays (HXRs), microwaves (MWs) and occasionally γ-rays in solar flares are believed to be generated from non-thermal processes. The HXR and MW observations provide the most direct information on non-thermal electrons. HXRs below $\sim$100 keV are primarily emitted by electrons with energy below several hundred keV via bremsstrahlung radiation, whereas MWs above $\sim$10 GHz are emitted by electrons above several hundred keV via gyrosynchrotron radiation (e.g., Ramaty 1969; Brown 1971; Bastian 1999). Thus, observations from these two different frequency ranges complement each other and provide good diagnostics for energetic electrons from solar flares.

* Supported by the National Natural Science Foundation of China.

The nearly simultaneous spikes in major HXR and MW bursts have generally been considered to be evidence that indicates the HXRs and MWs are emitted from the same group of electrons interacting with ambient plasma and a magnetic field. However, time delays from several milliseconds to dozens of seconds have been observed among MWs and HXRs (e.g., Cornell et al. 1984; Lu & Petrosian 1990; Lee & Wang 2000). These time delays are concerned with two independent phenomena. One is the energy dependent time delays in X-rays with higher energy peaks retarding the lower energy peaks, and the other is the frequency dependent time delays in MWs with higher frequency peaks preceding the lower frequency MWs (e.g., Takakura et al. 1983; Aschwanden et al. 1997; Lee & Wang 2000). The former can be explained in terms of magnetic trapping or the acceleration process (see, Cornell et al. 1984; Lu & Petrosian 1990; Aschwanden et al. 1997). The latter can be understood in terms of a few models, for example, (i) the collisionless conduction front model, and (ii) directional particle acceleration by shock waves in a suitable magnetic field and electron spectrum (e.g., Wiehl et al. 1980; Kaufmann et al. 1982, 1983; Berg-Hanssen et al. 1984; Brown et al. 1983; Costa & Kaufmann 1983; Takakura et al. 1983; Gu & Li 1986).

The time differences in the maxima of MW burst fluxes are essential factors for understanding the evolution of energetic electrons in solar flares. They are also important for diagnosing plasma conditions in the source regions, particularly together with simultaneous HXR observations. Many works were investigated in the 1970s through the 1990s, when only X-ray remote-sensing data from the Hard X-ray Imaging Spectrometer (HXIS, van Beek & Schrijver 1980) onboard the *Solar Maximum Mission* and the Solar X-ray Telescope (SXT, Tanaka 1983) onboard the *Hinotori* satellite to image below 40 keV were available. These early observations were limited in terms of both number of energy channels and spatial resolution (e.g., Lin et al. 1981; Anderson et al. 1978). Without high-resolution spatial data, it was difficult to distinguish whether the HXR and MW sources were co-spatial or not. Now that both high-resolution spatial and temporal HXR and MW observations are available, it is possible to study this problem further. For this purpose, we investigated the 2005 August 22 flare event (00:54 UT) using HXR and MW observation data from the *Reuven Ramaty High Energy Solar Spectroscopic Imager* (*RHESSI*) and the Nobeyama Solar Radio Observatory (NRO). We chose this flare event because its non-thermal emission profiles expose quasi-periodic pulsations, which are different from other flare events. There are already some papers on this event (e.g., Li & Gan 2008; Reznikova et al. 2010; Reznikova & Shibasaki 2011; Lugaz et al. 2011). All these works did not include comparison studies on variations of observational flux in the HXRs and MWs. Hence, in this paper, we mainly focus on this issue and carry out some qualitative analysis. We first present a comparative study of the spatially integrated non-thermal emissions and spatially resolved non-thermal emissions of the flare in Section 2. Then we analyze the observed phenomena in Section 3. Finally, we summarize our conclusions in Section 4.

2 OBSERVATIONS

We analyzed the solar flare which took place on 2005 August 22 (00:54 UT) from the active region (NOAA 10798) in the southwest heliographic coordinates (S12°, W49°) of the Sun. It was a medium strength flare (M2.6 on the *GOES* scale) that lasted about an hour.

Figure 1(a) shows the light curve of HXRs at 25–50 keV and MWs at 17 GHz and 35 GHz, (b) their morphology during the first emission peak and (c) also the magnetic configuration before the first burst. *RHESSI*[1] (e.g., Lin et al. 2002) was in the shadow of the Earth until about 01:02 UT and hence no X-ray data were available before this time. The HXR light curve clearly exhibits a damped quasi-periodic oscillation and the MW light curve follows corresponding spikes with increasing fluxes instead of undergoing a quasi-periodic oscillation.

[1] The website of *RHESSI* is *http://sprg.ssl.berkeley.edu/ tohban/browser/?show=grth+qlcr*

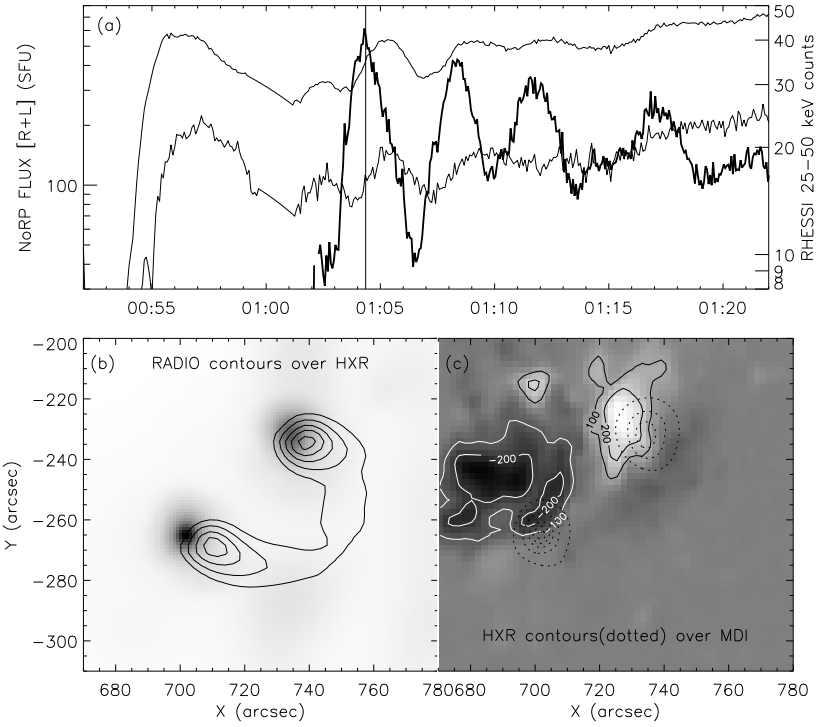

Fig. 1 (a) The light curves from the Nobeyama Radio Polarimeters (NoRP) at 17 GHz (*upper thin line*) and 35 GHz (*lower thin line*), and *RHESSI* 25–50 keV counts (*thick line*). The vertical line (01:04:20 UT) shows the time HXR and MW images are acquired; (b) Nobeyama Radio Heliograph (NoRH) 34 GHz contours (levels: 10%, 30%, 50%, 70% and 90%) for 01:04:21–01:04:22 UT, are overlaid on the *RHESSI* 25–50 keV PIXON image (01:04:10–01:04:30 UT); (c) the *SOHO*/MDI longitudinal magnetic field image (00:00:29 UT) with contour levels of –200, –100 (*white*) and 100, 200 (*black*). The *RHESSI* 25–50 keV HXR dashed contours (levels: 20%, 40%, 60% and 80%) are overlaid to mask the footpoints of the flaring loop.

2.1 NoRP Data

The flare frequency spectrum in Figure 2 reconstructed with NoRP (e.g., Nakajima et al. 1985) data at 01:05:03 UT shows a typical gyrosynchrotron shape with the turnover frequency or peak frequency $f_{\rm p}$ ∼9.7 GHz and negative slope over $f_{\rm p}$. The peak frequency $f_{\rm p}$ during the flare period is observed to be ≤10 GHz. Emissions below $f_{\rm p}$ are in the optically thick part where plasma emissions are efficient, and emissions above $f_{\rm p}$ are in the optically thin part where gyrosynchrotron emissions contribute most (e.g., Guidice & Castelli 1975; Melnikov et al. 2008).

Since corresponding emission peaks are shown in both HXRs and MWs, we can study the time association among the corresponding peaks. The vertical lines in Figure 3 mark the peak times of different frequencies. We found that there are significant time delays between peaks of MWs and HXRs. In the first peak, it is clear that there exist frequency dependent delays such that the higher frequency peaks precede the lower frequency peaks (< 17 GHz).

The refined result is exhibited in Figure 4, and the correlation coefficient between frequencies and time delays is $R = -0.98$ with a confidence level of 99%. The MW peaks keep getting flatter

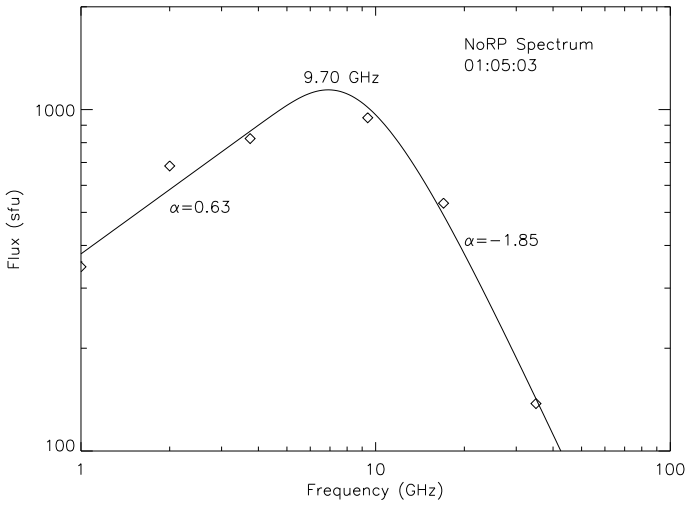

Fig. 2 The flare frequency spectrum reconstructed from NoRP data at 01:05:03 UT, with a positive slope below 9.7 GHz and a negative slope above it.

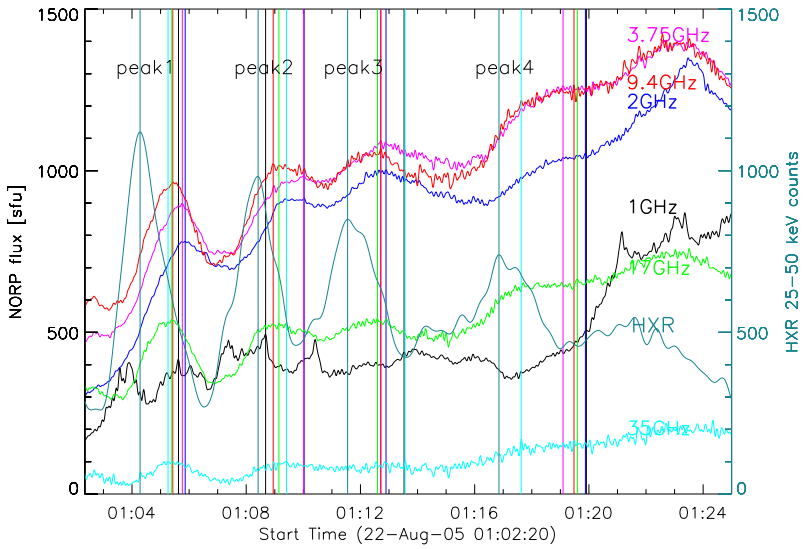

Fig. 3 The MW flux time profiles at six different frequencies (1.0, 2.0, 3.75, 9.4, 17.0 and 35 GHz) are exhibited in different colors. The vertical lines mark each peak time with corresponding colors. The HXR 25–50 keV flux time profile is also shown.

with a steep rising phase and a gradual decaying phase, which makes it difficult to pinpoint the peak times, but it is still clear in the optically thick part below 9.4 GHz that the higher frequencies precede the lower frequencies (see Fig. 3). For higher frequencies in the optically thin part, the lower frequencies seem to precede the higher frequencies, but it is not yet very clear.

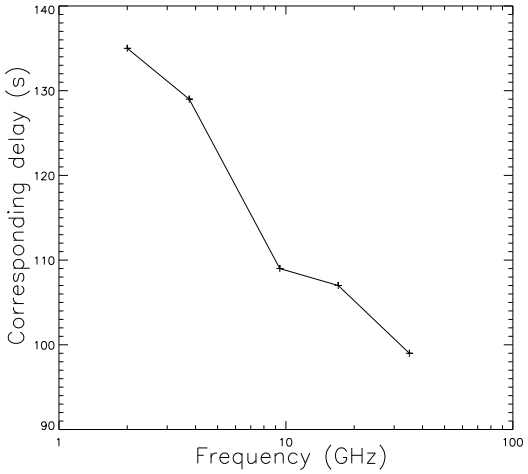

Fig. 4 The peak time delay between MWs and HXRs at five different MW frequencies (2.0, 3.75, 9.4, 17.0 and 35 GHz) during the first peak based on the observed data shown in Fig. 3. The horizontal axis denotes the frequencies and the vertical axis denotes the corresponding delay time in seconds. The correlation coefficient for the relation between frequency and time delay is –0.979102.

2.2 *RHESSI* and NoRH Data

2.2.1 MW and HXR images of footpoint sources

Both *RHESSI* and NoRH have superior spatial resolution, which makes it possible to distinguish different sources. However, locating the coordinates of the HXR and MW sources is not a simple task. It is difficult to determine the heliographic coordinates of the HXR and MW sources from an image acquired over a short time scale (see Fig. 1(b)). Moreover, coordinates of the NoRH images are generally found by fitting the position of the quiet solar disk, but this is not always feasible when the flare flux greatly exceeds the disk flux. Therefore, when the uncertainties in computations of positions on the solar disk are large, the positional accuracy of the NoRH images is poor. They can also suffer from relative shifts (e.g., Kundu et al. 2009). Under this consideration, we chose the areas with size $20'' \times 20''$ from NoRH images around the two footpoints, and selected the position with the peak flux as the center of the source every second from 01:02:01 UT to 01:15:01 UT. We then constructed a series of sources that are modeled as Gaussian distributions with the same intensity and a sigma of R (where R is the radius of the footpoint source that is considered to be a round area in which the intensity is larger than 70% of the peak, see Fig. 5(a)) and merged them together. Finally, we chose the centroids of the whole source to be the positions of the source, which are shown with white crosses in Figure 5(b). The HXR source positions are shown as black crosses in Figure 5(b), which are regarded as the centroids of the 50% contour of the *RHESSI* image acquired from 01:02:40 UT to 01:14:40 UT. The distances between HXR and the artificial MW footpoints are quite significant, and MW sources are much higher than HXR sources.

2.2.2 Emissions from different sources

Based on spatially resolvable observations from *RHESSI* and NoRH, we further studied the relative timing of HXR and MW emissions from different sources. We retrieved fluxes from two selected

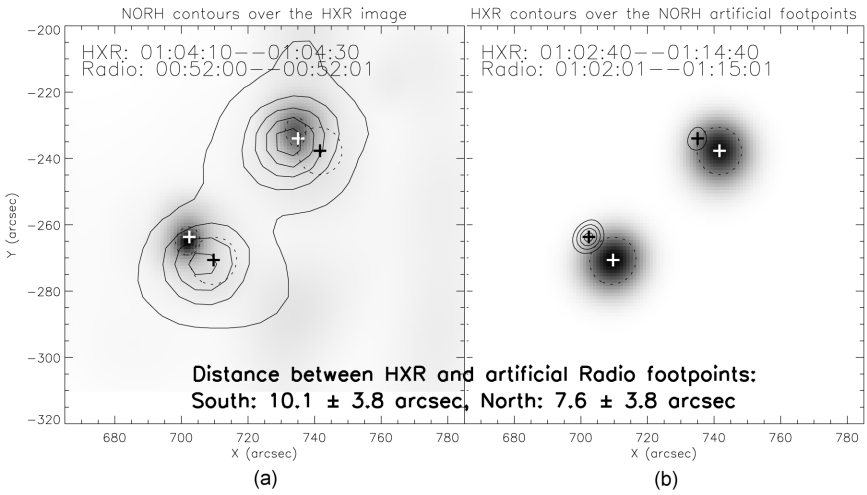

Fig. 5 (a) The contours from 00:52:00–00:52:01 UT NoRH 17 GHz (levels: 10%, 30%, 50%, 70% and 90%) are overlaid on the *RHESSI* 25–50 keV image. Cross symbols mark the centroids of the source regions. (b) The contours from *RHESSI* HXR 25–50 keV (levels: 30%, 50%, 70% and 90%) from 01:02:40 UT to 01:14:40 UT, made with the PIXON algorithm for grids 3F–9F except for 7F, are overlaid on an image of the NoRH 34 GHz artificial footpoints with a contour denoting 50% (*dashed*). Cross symbols are drawn at the same positions as in (a) but in the opposite color.

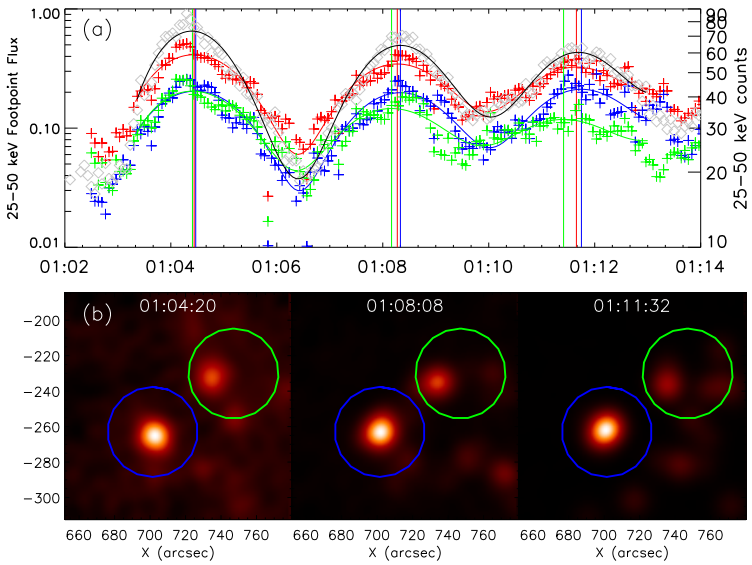

Fig. 6 (a) the time profile of *RHESSI* 25–50 keV fluxes from the whole active region is shown with red pluses and a fitted line, that from the south footpoint is shown with blue crosses and a fitted line and that from the north footpoint is shown with green crosses and a fitted line; diamonds and a fitted line show the total counts. The vertical colored lines indicate the corresponding peak times of the fitted lines; (b) the 25–50 keV images are made with the CLEAN algorithm for grids 3F–9F except 7F at each peak time marked by vertical red lines. The blue and green circles in the figure denote the south and north regions in which the photons are accumulated.

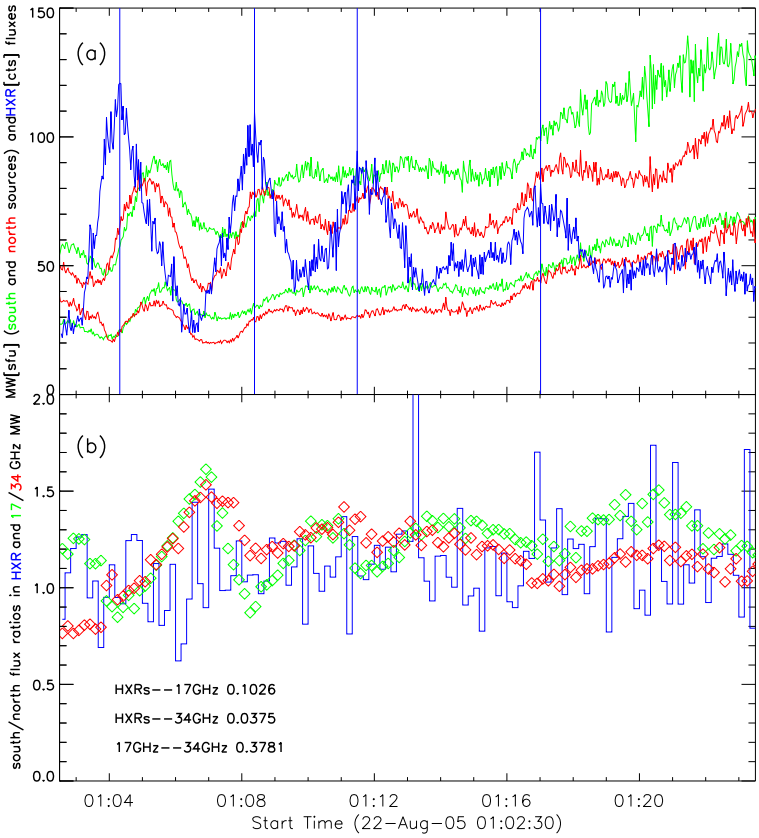

Fig. 7 (a) the blue line is the time profile of HXR 25–50 keV flux counts (divided by 10) from the whole active region; the green and red lines are fluxes from the south and north source areas respectively where the emission intensity is larger than 60% of the maximum at 17 GHz (stronger one) and 34 GHz (weaker one); (b) the flux ratios of the south source divided by the north source of HXRs (25–50 keV) and MWs (17 GHz and 34 GHz) are shown in the blue histogram, and green and red diamonds, respectively. The correlation coefficients of ratios between HXRs and 17 GHz, HXRs and 34 GHz, and 17 GHz and 34 GHz are given in the bottom left.

circular areas for HXR 25–50 keV footpoint sources (see Fig. 6). The vertical lines indicate the peak time for the fitted line with a damped periodic function (Li & Gan 2008). For MW emissions from different sources, we integrated the fluxes from the area in which the intensities were larger than 60% of the peak intensity around the north and south footpoints.

In this regard, Figure 7(a) demonstrates that the peak times at the same frequency of the two different sources are different, and their cross-correlation (which we do not present here) shows that emission from the north source precedes that from the south by nearly 10 s. As a next step, we calculated the flux ratios of the south source over the north source in HXRs (25–50 keV, blue) and MWs (17/34 GHz, green/red) as shown in Figure 7(b). The correlation coefficients of the ratios between MWs and HXR are all positive, however, the confidence levels of the first two are very low, so they can be regarded as being unrelated, unlike the 17 GHz versus 34 GHz fluxes that have a confidence level of more than 99%.

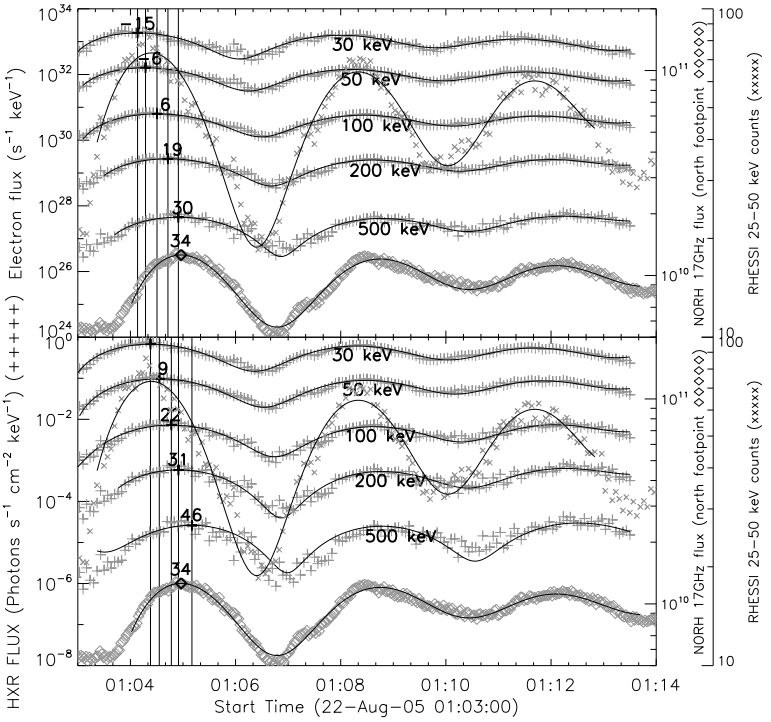

Fig. 8 *Top*: the electron fluxes (*pluses and fitted lines*) derived from fitting the single power-law electron thick-target model to the observed *RHESSI* HXR spectrum. The north footpoint 17 GHz MW fluxes (*diamonds and fitted lines*) and the 25–50 keV *RHESSI* counts (*crosses and fitted lines*) are also displayed. *Bottom*: the HXR fluxes derived from fitting the single power-law model to the *RHESSI* HXR spectrum. The vertical lines mark the peak times of different energies. The numbers around the first peak denote the delay time with respect to the 25–50 keV flux peak time.

2.2.3 Further analysis of observed HXRs and MWs

We derived the electron fluxes from the single power-law electron thick-target model to fit the *RHESSI* HXR photon spectrum and then extended the fit to include the HXR flux at higher energies. As the fitted HXR fluxes showed good periodicity, we fitted them with a quasi-periodic function (see Li & Gan 2008), and thus obtained the corresponding peak times for different energies (see Fig. 8). The vertical lines around the first peak indicate the peak times, and the north NoRH 17 GHz footpoint flux is shown for comparison. The peak time of the 17 GHz flux is located around the peak time for an electron flux of several hundred keV.

We further compared the spectral index and their time profiles. As shown in Figure 9, the vertical magenta lines indicate the times of the first peak fluxes for 17 GHz and 34 GHz MW obtained from NoRH data. The 17 GHz MW precedes the 34 GHz MW by 14 s but all tend to be retarding the peaks in HXRs. The green lines are the time profiles of MW spectral indices derived from NoRH 17 and 34 GHz fluxes ($\alpha = \ln(\mathrm{Flux}_{34\,\mathrm{GHz}}/\mathrm{Flux}_{17\,\mathrm{GHz}})/\ln(34\,\mathrm{GHz}/17\,\mathrm{GHz})$). It is observed that the index varies almost synchronously with the HXR 25–50 keV flux even in some structures that span a short time scale, maintaining a strong correlation coefficient of 0.81 with a confidence level

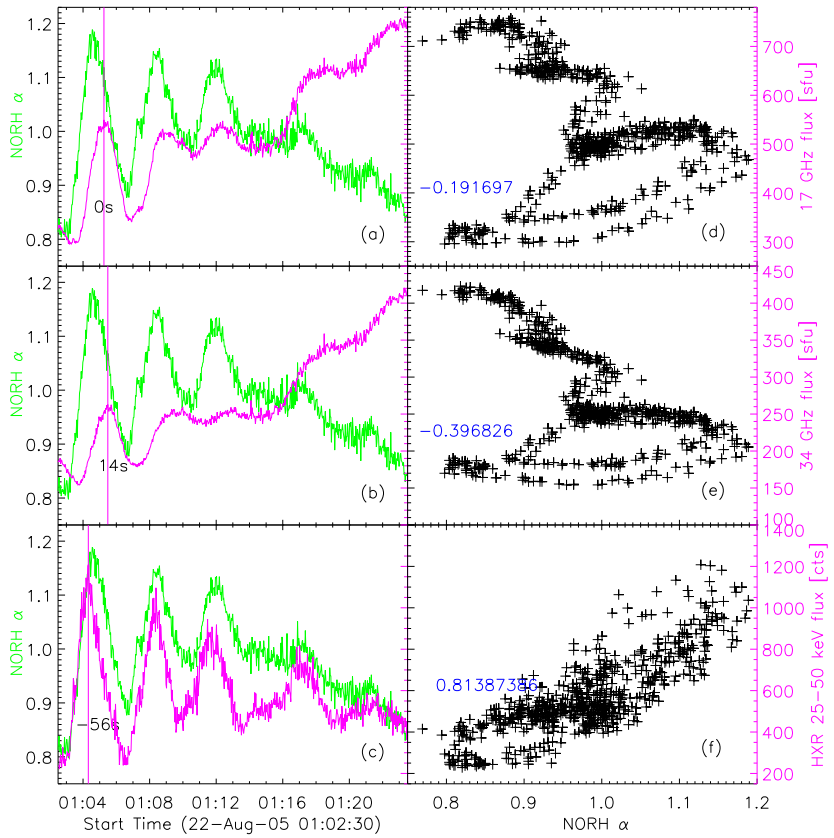

Fig. 9 The green lines denote the MW spectral index time profile derived from NoRH 17 GHz and 34 GHz observations. The magenta lines indicate the relative fluxes of NoRH 17 GHz (a), NoRH 34 GHz (b) and flux counts of HXR (c). The vertical lines mark the peak times of fluxes and the corresponding numbers in the panels denote their corresponding timings. The right panels show the correlations of the MW spectral index with fluxes at NoRH 17 GHz (d), NoRH 34 GHz (e) and HXR (f). The corresponding correlation coefficients are shown in blue.

of 99.9% (see Fig. 9(c) and (f)). The correlations in Figure 9(d) and (e) are not very clear because the relations changed during different time periods spanned by those peaks.

3 DISCUSSIONS

3.1 Quasi-Periodic Pulsations

Earlier, Li & Gan (2008) concluded that this flare event exhibited very good quasi-periodic pulsation in the temporal profile of HXR emission. For this periodic emission, Reznikova et al. (2010) found that the clearly-visible MW loop as well as HXR footpoints during the flare followed the direction and orientation of the post-flare EUV arcade, and hence they regarded this as evidence that the successive emission peaks on the time profile of this flare are due to magnetic reconnection occurring in different parts of the arcade, not in the same magnetic loop. Furthermore, Reznikova & Shibasaki

(2011) suggested that the second standing harmonics of the slow magnetoacoustic mode generated by an initial impulsive energy deposition worked as a trigger for the repeated energy releases.

3.2 Frequency Dependent Delays of MWs

The frequency dependent delays are related to the temporal variation of the MW spectrum with a simultaneous increase and decrease at these frequencies (Takakura et al. 1983). This situation can be attributed to the faster decrease in the number of energetic electrons, which emit MWs at higher frequency in the optically thin phase, and a simultaneous extension of the acceleration region towards upper layers with a relatively weak magnetic field to increase the flux at lower frequencies in the optically thick phase (Takakura 1972). For this flare, it is clear that below 9.4 GHz, the higher frequencies precede the lower frequencies as shown in Figure 3. But for emission from frequencies higher than 9.4 GHz, the fluxes are relatively weak, as shown in Figure 3 for 17 GHz and 35 GHz. We therefore exploited the NoRH[2] (e.g., Nakajima et al. 1994) data instead of NoRP[3] data for the study of relative timing in the optically thin part, and found the 34 GHz emission had a delay of 14 s with respect to the 17 GHz in the first peak, as shown in Figure 9. These results indicate that the higher frequency MWs precede the lower frequency MWs in the optically thick part below 9.4 GHz, and they become reversed in the optically thin part.

Regarding the frequency dependent delays in the optically thick part, Wiehl et al. (1980) proposed that the MW time delays at lower frequencies were due to the upward movement of the conduction front (Brown et al. 1979) at the ion-sound speed of 900 km s^{-1} and the rise time of different frequencies was determined by the time it took for the front to travel through the corresponding emitting layer. Along the same vein, Takakura & Scalise (1970) calculated the effective height at different frequencies in a model incorporating a dipole field, in which the main emissions arise from the second harmonic mode of gyrosynchrotron emission. They suggest that it is about 8×10^4 km at 1 GHz, and it decreases with frequency to 3×10^4 km at 9.4 GHz and then increases with frequency to about 4.5×10^4 km at higher frequencies (see fig. 4 in Takakura & Scalise (1970)). That is to say, in this model (see figs. 1 and 2 in Takakura & Scalise (1970)) it takes tens of seconds for the conduction front to travel through the emitting layers, and the flux density around 9.4 GHz peaks earlier than all other frequencies. In comparison with 9.4 GHz, 1 GHz peaks 55 s later and high frequency emissions such as that around 100 GHz peak 17 s later. In addition to this explanation, Brown et al. (1983) suggested a dissipative thermal mode with a multiple kernel model in which many single annihilation regions of varying magnetic field strength, each with a short lifetime, are continuously produced throughout the burst to explain the long time delays ($>$10 s).

3.3 Differences in Peak Times between HXRs and MWs

Long time delays between MWs and HXRs (Fig. 3) are much longer than the lag due to magnetic trapping (e.g., Lu & Petrosian 1990; Minoshima et al. 2008). However, such a long time delay could be simply caused by accelerating higher energy electrons later. In this respect, we assume that the lower energy electrons were injected into the loop system and generated HXRs but there were few electrons accelerated to hundreds of keV to generate MWs until dozens of seconds later. Inspired by this assumption, we derived the electron fluxes by fitting the *RHESSI* HXR photon spectrum, and then extended the results to the HXR flux at higher energies (as seen in Fig. 8). As is well known, for a relativistic electron circling around a magnetic field, the most powerful gyrosynchrotron emission is generated at a frequency of $W = \gamma^2 \Omega_e$ (Tucker 1975), where γ is the Lorentz factor and Ω_e is the cyclotron frequency. In this respect, we can simply estimate the energy E of electrons responsible

[2] Nobeyama Radio Heliograph (NoRH): *http://solar.nro.nao.ac.jp/norh/*

[3] Nobeyama Radio Polarimeter (NoRP): *http://solar.nro.nao.ac.jp/norp/*

for the MW emission at a frequency of W as

$$E = (\gamma - 1)\, m_e C^2 = (\sqrt{W/\Omega_e} - 1)\, m_e C^2 = (\sqrt{F/n\Omega_e} - 1) \times 511 \text{ keV}\,,$$

where F is the observed emission frequency and n is the harmonic number. We fitted the MW spectrum in Figure 2 with the nonthermal gyrosynchrotron emission program in Solar Software and estimated that the average magnetic field of the emission source is around 250 G. The cyclotron frequency can then be taken as $\Omega_e = eB/2\pi m_e C = 0.7$ GHz. In this way, if the harmonic number of most observed MW emissions is 10, we can speculate that the electrons with energies 280 keV and 610 keV are the main electrons responsible for $F = 17$ GHz and $F = 34$ GHz MW emissions, respectively. This indicates that it took 14 s (see Fig. 9) to accelerate an electron with energy 280 keV to an energy of 610 keV during the first peak. This is consistent with the plot shown in Figure 8, suggesting that quite a slow evolution took place in the acceleration process.

For this event, the loop-top source emission flux changed very gradually without showing any emission peaks, and did not exhibit the same quasi-periodic pulsation behavior as the footpoint sources did. This characteristic has been illustrated by Reznikova et al. (2010) in the context of the electron acceleration model in a collapsing magnetic field (e.g., Somov & Kosugi 1997; Bogachev & Somov 2005). They suggested that, during these peaks, non-thermal electrons were injected along the loop axes like beams passing swiftly through the loop apex, generating emission with very small intensity. In this regard, Somov & Kosugi (1997) and Bogachev & Somov (2005) suggested that the contracting local trap can serve as an efficient accelerator for relativistic energies via the first-order Fermi and betatron acceleration mechanisms. However, the typical lifetime of the contracting local trap is about 10 s, which is much shorter than the observed time difference between the HXRs and MWs in this flare. To make the collapsing magnetic trap physically realistic, the outflow velocity (typically 1400 km s^{-1}) needs to be much slower, but the speed of local fast magnetoacoustic waves is about 1000 km s^{-1}, and when the former becomes slower than the latter, the model would break down and a new progressive acceleration model that operates over a long time is required.

It is necessary to mention that the HXR emissions over 50 keV were very weak, which means that there were few high energy electrons directly penetrating into the footpoints. Most of the high energy electrons were supposed to be injected with a large pitch angle so that they could be trapped to generate MW emissions. However, this contradicts the assumption of a small pitch angle that is needed to explain the missing emission peaks from the loop-top source (Reznikova et al. 2010).

3.4 The Relationship between Spectral Index and HXR Flux

Considering that the time delays discussed above might be related to the spectral evolution of electrons generating HXR and MW emissions, we compared the spectral index with their time profiles (see Fig. 9). From Figure 9(a) and (b), it is evident that the spectrum of MWs in the optically thin part is becoming harder and harder over each flux peak. This is consistent with the fact that the higher frequency peaks are delayed with respect to the lower frequency ones.

In Figure 9(c), the NoRH MW spectral index strongly anticorrelates with the HXR flux, suggesting that the high energy electrons emitting MWs underwent a hard-soft-hard (HSH) process with respect to the HXR flux over every peak. Song et al. (2011) and Huang & Li (2011) suggested that the HSH variation of MWs could be accounted for if there is a strong trapping effect of high energy electrons. Since the higher the energy of electrons becomes, the longer they might be trapped, the spectrum of trapped electrons becomes harder and harder. Every time newly released electrons are injected into the loop, the spectrum of trapped high energy MW emitting electrons becomes soft, and a simultaneous flux of HXRs are emitted by the lower energy electrons penetrating into footpoints. If this was what indeed occurred during the periodic pulsations of this flare, both the higher and lower energy electrons should be released simultaneously and no progressive acceleration process

was required. In this case, however, the long delays discussed in Section 3.2 and 3.3 turn out to be problematic and further studies are required.

3.5 Differences in Peak Times of Emissions from Different Sources

Since the flux from the loop-top source does not expose the corresponding peaks like the footpoint sources do, here we only consider how the times between the two footpoint sources are related. As observed (Figs. 6 and 7) the HXR emissions from the two footpoints are relatively simultaneous within the measurement error, but the MW emissions are not synchronous with each other. This excludes the possibility of different locations for the sources causing this delay, because even if the sources are displaced by 10 000 km along the line of sight, a difference in arrival time of only 33 ms would be expected. Considering that the time differences might be related to variations in the magnetic field around the emission sources, we calculated the flux ratios of south to north in 17/34 GHz MWs and HXRs. The MW ratios display oscillations with four weak peaks but the HXR ratio changes very quickly around 1.0 because of the short lifetime of electrons that emit HXR. Since the stronger the magnetic field becomes, the higher the intensity of MW emission and the weaker the HXR emission that would be generated due to the loss cone effect, the flux ratios of MWs and HXRs are expected to be anticorrelated. However, in Figure 7, the correlation coefficients of the flux ratios of MWs and HXRs are all positive, so the possibility that variations in the magnetic configuration caused the above delay between different sources should be excluded. It might be related to the pitch angle distribution of injected electrons, but more detailed analysis is needed to confirm this.

4 SUMMARY AND CONCLUSIONS

We studied both HXR and MW emissions of the solar flare SOL2005-08-22T00:54 with *RHESSI* and NoRH/NoRP data. The 25–50 keV HXRs exhibited very good quasi-periodic pulsations, which have been considered to be a result of repeated magnetic reconnection driven by the second standing harmonics of the slow magnetoacoustic mode (e.g., Li & Gan 2008; Reznikova et al. 2010; Reznikova & Shibasaki 2011). The MWs followed corresponding emission peaks with larger and larger intensity due to electron trapping of the converging magnetic field. With the four corresponding flux peaks of HXRs and MWs, we studied their relative timings, and found significant frequency dependent time delays in MWs and energy dependent time delays in HXRs. For a better understanding of the delays between different frequencies, we discussed the conduction front model suggested by Wiehl et al. (1980) and also the thermal model by Brown et al. (1983). Regarding the energy dependent delays, we derived the electron fluxes from observed HXR data and found that the higher energy electrons were delayed with respect to the lower energy electrons. We speculated that this can be accounted for if higher energy electrons are accelerated later than lower energy electrons. We discussed the collapsing magnetic trap model suggested by Reznikova et al. (2010) as the accelerator but concluded that the lifetime of the local trap was too short to generate the hypothetical long acceleration process in this event. Considering the relationship between the variation of the electron spectrum and the emission delays, we further compared emission fluxes with the MW spectral index based on NoRH data. The strong anti-correlation between the NoRH spectral index and HXR flux suggests a simultaneous release of both lower and higher energy electrons occurred. Further work is required to distinguish which is the exact process that occurred in non-thermal electrons during this flare. Finally, we discussed the differences in peak time of the two footpoints, and noted that the discrepancy should not be a result of variations in the magnetic field.

Acknowledgements This work is supported by the National Basic Research Program of China (973 Program, 2011CB811402) and the National Natural Science Foundation of China (Grant Nos. 11233008, 11273065 and 11173063). Z. L. is grateful to Dr. S. Liu for useful discussions.

References

Anderson, K. A., Kane, S. R., Primbsch, J. H., et al. 1978, IEEE Transactions on Geoscience Electronics, 16, 157
Aschwanden, M. J., Bynum, R. M., Kosugi, T., Hudson, H. S., & Schwartz, R. A. 1997, ApJ, 487, 936
Bastian, T. S. 1999, in Proceedings of the Nobeyama Symposium, eds. T. S. Bastian, N. Gopalswamy, & K. Shibasaki, 211
Berg-Hanssen, E. T., Kaufmann, P., Reichmann, E. J., et al. 1984, Sol. Phys., 90, 41
Bogachev, S. A., & Somov, B. V. 2005, Astronomy Letters, 31, 537
Brown, J. C. 1971, Sol. Phys., 18, 489
Brown, J. C., MacKinnon, A. L., Zodi, A. M., & Kaufmann, P. 1983, A&A, 123, 10
Brown, J. C., Spicer, D. S., & Melrose, D. B. 1979, ApJ, 228, 592
Cornell, M. E., Hurford, G. J., Kiplinger, A. L., & Dennis, B. R. 1984, ApJ, 279, 875
Costa, J. E. R., & Kaufmann, P. 1983, A&A, 119, 131
Gu, Y.-M., & Li, C.-S. 1986, in NASA Conference Publication, 2449, NASA Conference Publication, eds. B. R. Dennis, L. E. Orwig, & A. L. Kiplinger, 91
Guidice, D. A., & Castelli, J. P. 1975, Sol. Phys., 44, 155
Huang, G., & Li, J. 2011, ApJ, 740, 46
Kaufmann, P., Costa, J. E. R., Dennis, B. R., et al. 1983, Sol. Phys., 84, 311
Kaufmann, P., Costa, J. E. R., & Strauss, F. M. 1982, Sol. Phys., 81, 159
Kundu, M. R., Grechnev, V. V., White, S. M., et al. 2009, Sol. Phys., 260, 135
Lee, C.-Y., & Wang, H. 2000, Sol. Phys., 195, 149
Li, Y. P., & Gan, W. Q. 2008, Sol. Phys., 247, 77
Lin, R. P., Schwartz, R. A., Pelling, R. M., & Hurley, K. C. 1981, ApJ, 251, L109
Lin, R. P., Dennis, B. R., Hurford, G. J., et al. 2002, Sol. Phys., 210, 3
Lu, E. T., & Petrosian, V. 1990, ApJ, 354, 735
Lugaz, N., Downs, C., Shibata, K., et al. 2011, ApJ, 738, 127
Melnikov, V. F., Gary, D. E., & Nita, G. M. 2008, Sol. Phys., 253, 43
Minoshima, T., Yokoyama, T., & Mitani, N. 2008, ApJ, 673, 598
Nakajima, H., Sekiguchi, H., Sawa, M., Kai, K., & Kawashima, S. 1985, PASJ, 37, 163
Nakajima, H., Nishio, M., Enome, S., et al. 1994, IEEE Proceedings, 82, 705
Ramaty, R. 1969, ApJ, 158, 753
Reznikova, V. E., Melnikov, V. F., Ji, H., & Shibasaki, K. 2010, ApJ, 724, 171
Reznikova, V. E., & Shibasaki, K. 2011, A&A, 525, A112
Somov, B. V., & Kosugi, T. 1997, ApJ, 485, 859
Song, Q., Huang, G., & Nakajima, H. 2011, ApJ, 734, 113
Takakura, T. 1972, Sol. Phys., 26, 151
Takakura, T., Ohki, K., Kosugi, T., Enome, S., & Degaonkar, S. S. 1983, Sol. Phys., 89, 379
Takakura, T., & Scalise, E. 1970, Sol. Phys., 11, 434
Tanaka, Y. 1983, Sol. Phys., 86, 3
Tucker, W. 1975, Radiation Processes in Astrophysics (Cambridge, Mass., MIT Press), 320
van Beek, H. F., & Schrijver, H. 1980, Ruimtevaart, 29, 225
Wiehl, H. J., Schochlin, W. A., & Magun, A. 1980, A&A, 92, 260